Renewable and Sustainable Energy Reviews 16 (2012) 4809–4817

Contents lists available at SciVerse ScienceDirect

Renewable and Sustainable Energy Reviews

journal homepage: www.elsevier.com/locate/rser

Integral analysis of rotors of a wind generator

Rafael Romão da Silva Melo*, Aristeu da Silveira Neto

Federal University of Uberlândia, Department of Mechanical Engineering, Fluid Mechanic Laboratory, Campus Santa Mônica, Bloc 5P, Uberlândia, Minas Gerais, Brazil

ARTICLE INFO

Article history:
Received 25 November 2011
Received in revised form
28 March 2012
Accepted 31 March 2012
Available online 27 June 2012

Keywords:
Wind turbine
Wind energy
Integral analysis

ABSTRACT

The world's population needs new sources of energy, especially those that are clean and renewable. This paper provides a brief introduction to wind energy and the types of existing turbines, which are classified using the orientation of the rotation axis. Subsequently, an integral analysis is performed for vertical axis turbines. The known variables are the wind speed, the type of blade, the radius of the rotor and the angular velocity. The fluid velocity and the angle of attack on the blade are subsequently determined. From these two results, the lift and drag forces acting on the blades for each position of the rotor are calculated. The resultant torque and power generated are also calculated to evaluate the turbine power coefficient. Due to the rotation and the robustness of this type of turbine, a distortion in the flow direction occurs in its vicinity. The flow is modeled on a control volume, which is defined based on the variation in the wind direction.

Contents

1. Introduction

Humanity faces a major challenge in meeting energy demands while avoiding damage to the environment. Energy transported by the wind is part of the solution to this problem. Wind energy is renewable and does not cause any harm to the environment, thereby enabling the generation of clean electricity. In addition to this advantage, the cost of wind energy compared to the cost of conventional systems is already notably competitive [1]. Wind energy produces no pollutants in contrast to a thermal power plant that produces approximately 1 kg of carbon dioxide for each kWh produced.

The amount of energy available in wind varies with the seasons and the time of day, due to variations in wind speed. The topography and roughness of the soil also have considerable influence on the distribution of wind speeds in one given place. Moreover, the amount of energy extracted from the wind depends on the performance characteristics, time of operation and relative positions of the wind turbines.

Wind turbines are machines used to extract renewable energy by absorbing part of the wind's kinetic energy through an aerodynamic rotor. The wind causes the turbine blade to rotate around its axis, converting the wind's kinetic energy into mechanical power, which is subsequently converted into electrical power through an electrical generator.

The amount of electricity that can be generated using the wind depends on four main factors: the amount of air passing through the turbine, the rotor diameter, the type of blade and the performance of the system.

The use of large turbines emerged with the technology of the 1970s after the oil crisis, when tax incentives, mostly in California (USA), allowed investments in these systems. Large concentrations of turbines, called Wind Farms, emerged. After the removal of such

* Corresponding author. Tel.: +55 34 32394040 616; fax: +55 34 32394242.
E-mail addresses: faelromelo@gmail.com (R. Romão da Silva Melo), aristeus@mecanica.ufu.br (A. da Silveira Neto).

1364-0321/$ - see front matter © 2012 Elsevier Ltd. All rights reserved.
http://dx.doi.org/10.1016/j.rser.2012.03.070

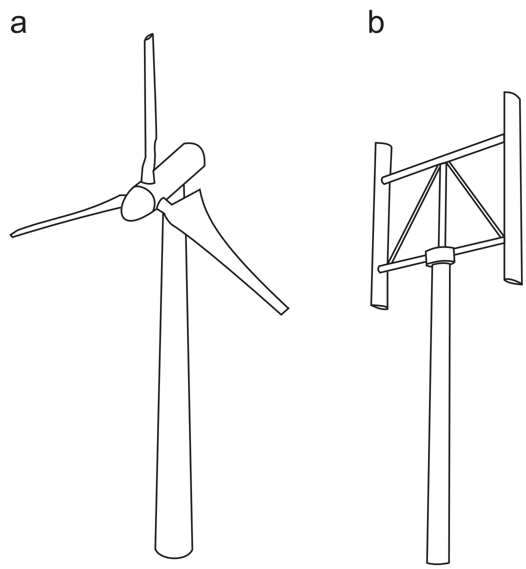


Fig. 1. (a) Horizontal axis wind turbines and (b) vertical axis wind turbines.

incentives, the pace of market expansion declined but resurged at the end of the 1990s. In this new millennium, there is a great concern for sufficient energy to meet the increasing consumption of both industrial and residential users.

A wind turbine is generally classified according to the orientation of its rotor axis [2]. The Horizontal Axis Wind Turbine (HAWT), shown in Fig. 1a, has blades that rotate in a plane perpendicular to the main direction of the wind. The Vertical Axis Wind Turbine (VAWT), shown in Fig. 1b, has blades that rotate in a plane parallel to the direction of the wind [3].

The HAWT is the most commonly used wind turbine in the market to produce energy on a large scale, but it requires a rotor axis positioned in the wind direction in order to achieve a higher performance efficiency, especially where there are frequent shifts in the wind direction. This type of turbine uses a tower to maintain the turbine components at an optimum height where wind speeds are higher. However, components may be situated up to 80 m high, creating some difficulty when performing inspections and maintenance.

The VAWT has the ability to capture wind from all directions without requiring steering systems to align the blades with the main wind flow. Instead of a tower, it is also possible to use support cables to provide structural stability, meaning that the elevation of the rotor can be lower and the turbine is smaller and less expensive to construct. With the blades at a lower elevation, the generator can be placed at the ground level, thereby facilitating inspection and maintenance [4]. Conversely, a larger base area for the turbine installation is required. This requirement is a major disadvantage in agricultural areas.

The first VAWT was the Panêmonas and worked with the principle of drag [2]. This wind turbine probably was originated in ancient Persia, China or Egypt. However, the modern VAWT, designed using modern aerodynamic concepts, was conceived by the Frenchman D.G.M. Darrieus in 1920 [2,5]. There are several geometric shapes of vertical axis wind turbines, which can be divided into three basic types, called Savonius type, Giromill type and Darrieus type.

The operation of the turbines of the type Savonius occurs through the drag force on its blades, which are two cups or half drums fixed to a central shaft in opposing directions. The wind reaches one of the drums and the drag generated on this causes the axis rotation. Then the next drum reaches the position occupied for the first, and the drag force causes the axis rotation too. This process continues all the time when the wind blows. Fig. 2a shows a Savonius turbine.

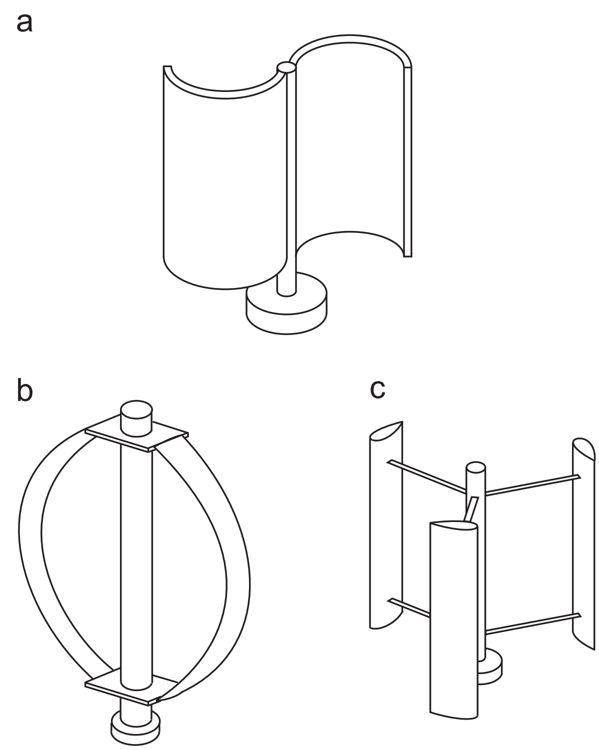


Fig. 2. (a) Savonius type VAWT, (b) Darrieus type VAWT, and (c) Giromill type VAWT.

The Darrieus turbine type is basically lift force driven wind turbine, whose long and flexible blades are fixed at their extremes and deformed, they take on a specific configuration, called a troposkien, which minimizes the bending stress in the blades. The Giromill type works like a Darrieus turbine, but uses straight edges and constant, became the case to be produced and transported, reducing costs. Fig. 2b and c shows a Darrieus and a Giromill turbine types, respectively.

A disadvantage of VAWTs is the fact that their blades, due to their rotation, constantly change their angles of attack relative to the wind direction, resulting in alternating and time-dependent forces. This property not only limits their efficiency but causes structural vibrations. Therefore, the choice of the blade geometry is of paramount importance when improving the performance of the turbines.

According to the literature there are three different methodologies to calculate the power generated by a vertical axis wind turbine using the stream-tube model: the single stream-tube model, the multiple stream-tube model, and the double-multiple stream-tube model. These models are based on equating the forces on the rotor blades to the change in fluid momentum in the flow direction through the rotor, and the difference between them is presented as follows.

The first model of the stream-tube methodology is the single stream-tube model, proposed by Templin [6]. This model is the simplest model because this assumes a constant disk velocity throughout the turbine. In other words the speed that reaches the blade is constant, independent of the angular position of this blade, because this model predicts a uniform flow for the entire cross-section (Fig. 3a). The forces on the airfoil blades are then computed, using this uniform velocity, then a certain error is generated, due to the fact that the speed is not constant in each angular position.

A new model was created in order to consider the variation in flow cross-section of the rotor, multiple stream-tube model,

developed by Strickland [7]. In this model a series of streamtubes are assumed to pass through the rotor (Fig. 3b). The same basic principles which were applied to the single streamtube are applied to each of the multiple streamtubes. By applying the momentum equation is each streamtube obtained the change in velocity that reaches the blade in each cross-section, yields a more realistic distribution of blade forces, so this model provides a better representation of what occurs in a vertical axis wind turbine.

Paraschivoiu [8] proposed a more sophisticated model called Double-Multiple Stream-Tube (Fig. 3c). As it uses two actuator disks placed in tandem into each tube of the multiple array, it can also predict differences between the upwind and downwind halves, so the results are more accurate.

The advancement of VAWTs depends on the success of current research projects and the performance of prototype systems under test. Vertical axis turbines are the focus of the present work.

2. Methodology

A physical model of the problem is first presented to determine and understand the variables that characterize the problem. Next, a mathematical analysis is presented. Finally, simulations are performed for various values of the parameters in order to find the best solution to this problem, i.e., maximum efficiency.

2.1. Physical model

Fig. 4 presents a simplified model of a vertical axis turbine projected on a horizontal plane, where a two-dimensional analysis is performed.

As air approaches a turbine, it is disturbed by the rotor, reducing its speed from the free stream wind speed (U_∞) to a lower speed U' [9,10]. Moreover, a distortion in the direction of the flow occurs in the vicinity of the turbine, mainly due to the rotation and robustness of this type of turbine. In other words, a streamline that tends to flow in one direction when approaching a turbine tends to turn in the same plane following the turbine. After passing through the turbine, this streamline resumes its original direction. Fig. 5 shows a magnified representation of what occurs near the turbine. This figure represents a control volume defined by planes 1 and 2 and by two chosen streamlines. The rotor is immersed in this control volume. A second control volume is delimited by planes 3 and 4 and by the same two streamlines. At

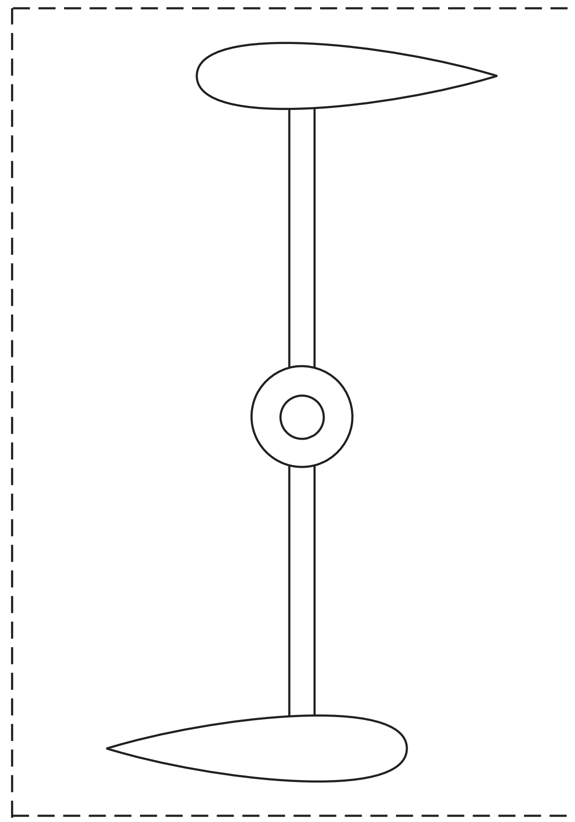


Fig. 4. Vertical axis turbine in a horizontal plane.

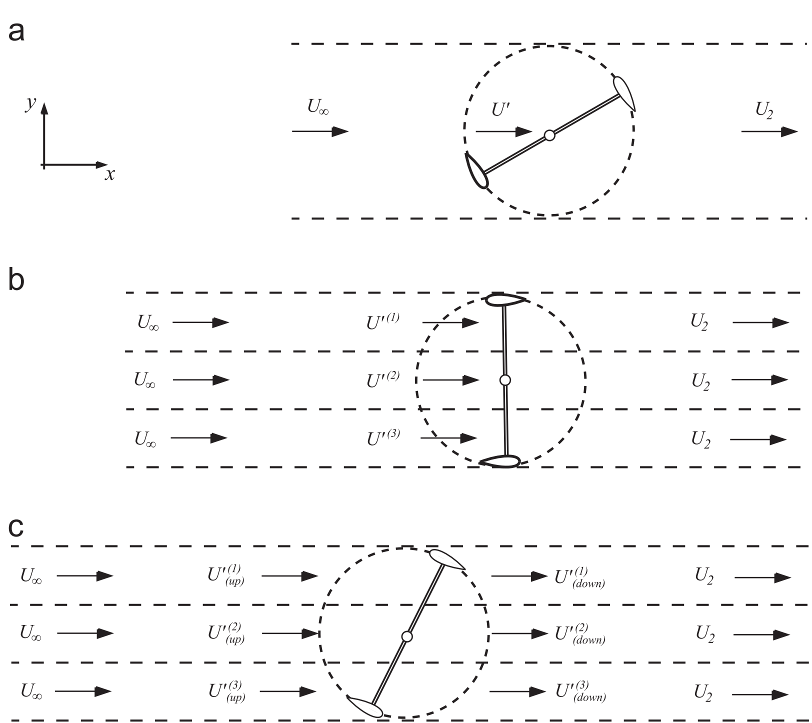


Fig. 3. Different types of stream-tube models.

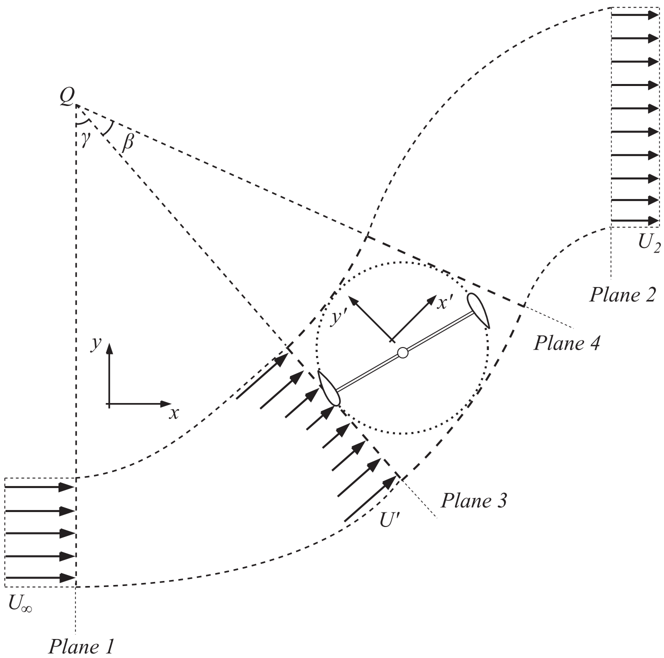


Fig. 5. Control volume for analysis of flow over the turbine.

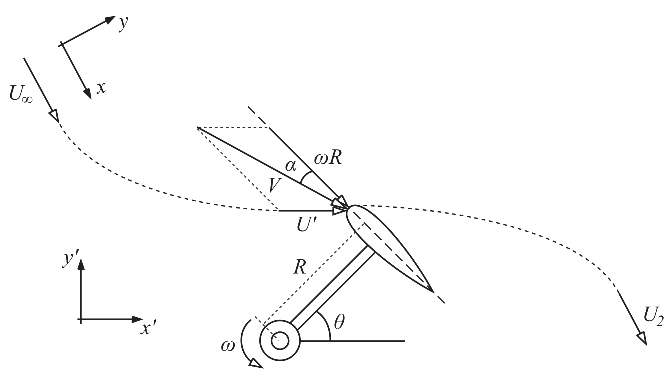


Fig. 6. Resultant velocity (V) and angle of attack (α) to a generic position θ.

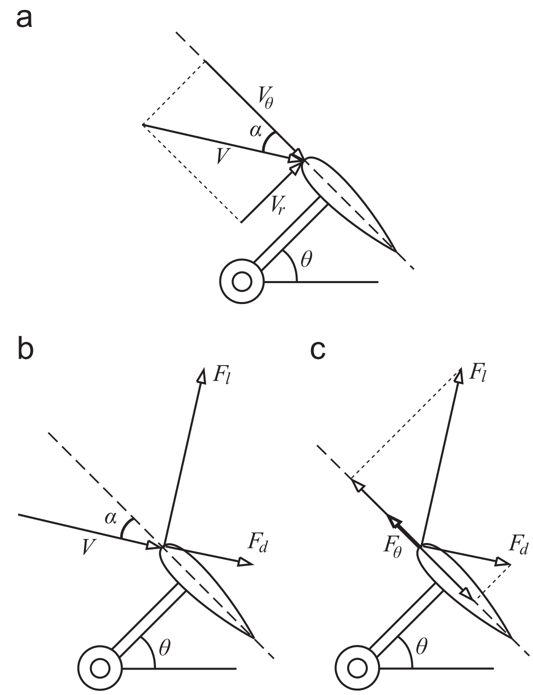


Fig. 7. (a) Resultant velocity on blade, (b) forces acting on the blade, and (c) resultant force in the direction of rotation.

plane 1 the wind speed is U_∞ (the free stream speed), and the pressure is the local atmospheric pressure. Plane 2 is considered to be sufficiently distant to have a uniform velocity (U_2) and a developed flow downwind of the rotor, where the pressure is also the atmospheric pressure. Planes 3 and 4 define the inlet and outlet flows over the turbine. Due to the speed reduction, it is expected that the pressure in plane 3 is greater than atmospheric pressure, and the pressure in plane 4 is lower than atmospheric pressure, due to the viscous effects inside the rotor.

A generic point Q was chosen to define the control volumes used in the analysis. From point Q, two lines were drawn tangent to the circle defined by the rotor, thereby defining planes 3 and 4. Close to this smaller control volume, we assume that the streamlines take the shape of an arc over the rotor with their centers at the point Q. For example, the smaller control volume around the rotor is bounded by two concentric arcs tangent to the rotor. The angle γ is formed by planes 1 and 3, and the angle β is formed by planes 3 and 4.

Fig. 6 is a diagram showing the wind velocity near the rotor (U'), the blade velocity (ωR) and the resultant velocity (V). The figure shows that the resultant wind velocity for any angle θ of the rotor is the sum of the wind speed (U') that strikes a blade and the relative velocity between the fluid and the rotating blade (ωR), where ω is the angular speed of the turbine and R is the radius of the rotor.

Knowing the resultant velocity of the fluid over the blade, the next step is to find the angle of attack (α), which is defined as the angle between the blade velocity (ωR) and the resultant velocity (V). The blade velocity (ωR) is placed over the central line of the blade (called the chord of the blade). Fig. 6 shows the resultant velocity and angle of attack (α) for a generic angle θ.

Using the resultant velocity (Fig. 7a) and the angle of attack, the forces acting on the blade are determined. These are the drag force (F_d) and the lift force (F_l) (Fig. 7b). By projecting these forces in the direction of the blade chord (Fig. 7c), the tangential force is determined. By multiplying the tangential force by the radius R of the turbine, the generated torque is determined. By multiplying this torque by the angular velocity, the generated power is obtained.

To finish the analysis, the remaining variables of the control volume must be determined, i.e., the U_2 velocity, pressures in positions 3 and 4 (P_3 and P_4, respectively) and the angles β and γ.

2.2. Mathematical model

The mathematical model for the described problem is given in the following steps, which are defined for a generic position θ ranging from 0 to 360°, thereby giving results for a full rotation of the rotor:

1: Estimate the wind velocity just before reaching the turbine (U') using the actual wind velocity (U_∞)

$$U' = U_\infty \tag{1}$$

2: Calculate the resulting fluid velocity on the blade using cylindrical coordinates. First, the velocity in the tangential direction (V_θ) and the velocity in the radial direction (V_r) are calculated

$$V_\theta = \omega R + U' \sin(\theta) \tag{2}$$

$$V_r = U' \cos(\theta) \tag{3}$$

Finally, the resulting velocity is calculated

$$V = \sqrt{(V_\theta)^2 + (V_r)^2} \tag{4}$$

3: The angle of attack α is calculated using the velocities in the radial and tangential directions

$$\alpha = \arctan \frac{V_r}{V_\theta} \tag{5}$$

4: The Reynolds number Re is calculated using Eq. (6) [11]

$$Re = \frac{\rho V c}{\mu} \tag{6}$$

where ρ is the fluid density, μ is the fluid dynamic viscosity and c is the blade chord. Because the Reynolds number and the angle of attack are known from experimental data [12], it is possible to determine the drag (C_d) and lift (C_l) coefficients for the blade in any position. These data are generated as follows: for different values of Reynolds number, C_l and C_d are calculated (from experimental data) for angles of attack ranging from 0 to 180°. Next, these data can be interpolated in order to determine C_d and C_l for any angle of attack and for any velocity.

5: Using the values of C_l and C_d for the resulting velocity and angle of attack, the coefficient in the direction of the axis x' ($C_{x'}$) is calculated, where x' is the direction of the air movement (Fig. 4). This value is obtained from the projection of C_l and C_d on x' [13]

$$C_{x'} = (C_d \cos\alpha - C_l \sin\alpha)\sin\theta + (C_d \sin\alpha + C_l \cos\alpha)\cos\theta \tag{7}$$

6: Using $C_{x'}$ calculated in the last step, the velocity of the wind that reaches the turbine is estimated and compared with the velocity estimated in step 1 to verify that these two velocities have the same value.
Analyzing the control volume between planes 1 and 2 (Fig. 4), we can say that the speed of the wind at the turbine (this step is called U'', which is the estimate of U' in each step) is the average between the input velocity (U_∞) and the output velocity (U_2) over the control volume [10]

$$U'' = \frac{U_\infty + U_2}{2} \tag{8}$$

The force in the x' direction is given by

$$F_{x'} = \frac{C_{x'} \rho U''^2 A}{2} \tag{9}$$

From a momentum balance [11], the force in the x' direction is also given by

$$F_{x'} = \dot{m}(U_\infty - U_2) \tag{10}$$

Isolating U_2 from Eq. (8) and using Eqs. (9) and (10), we have

$$U'' = \frac{U_\infty}{1 + C_{x'}/4} \tag{11}$$

7: The error between U' and U'' is given by

$$e = \left| \frac{U' - U''}{U''} \right| \tag{12}$$

If the error is larger than a given residue ε, one must return to step 2 and iterate assuming $U' = U''$ [7].
If the error becomes smaller than a given residue ε, the next step is taken.

8: Using the coefficients (C_l and C_d) for the correct speed, the lift force (F_l) and drag force (F_d) (Fig. 6b) are calculated [14]

$$F_l = C_l \tfrac{1}{2} \rho A V^2 \tag{13}$$

$$F_d = C_d \tfrac{1}{2} \rho A V^2 \tag{14}$$

9: With the correct values of F_l and F_d, the resulting forces in the normal and tangential directions are obtained

$$F_n = F_d \sin\alpha + F_l \cos\alpha \tag{15}$$

$$F_\theta = F_d \cos\alpha + F_l \sin\alpha \tag{16}$$

10: The next step is to calculate the generated torque

$$T = \sum_{i=1}^{N} \frac{F_\theta R}{2\pi} \Delta\theta \tag{17}$$

where $\Delta\theta = 2\pi/N$, and N is the number of discrete positions of the blade.

11: The generated power is given by

$$P = T\omega \tag{18}$$

12: Using the generated power, the power coefficient (C_p) is calculated [3,14–16]

$$C_p = \frac{P}{P_{max}} \tag{19}$$

where P_{max} is the maximum power that can be obtained from the wind [9,13]

$$P_{max} = \tfrac{1}{2} \dot{m} U_\infty^2$$

where $\dot{m} = \rho U_\infty A$ [9]. Therefore

$$P_{max} = \tfrac{1}{2} \rho A U_\infty^3 \tag{20}$$

In the next step, the remaining variables of the control volume are calculated.

13: The resultant force on the system in the smaller control volume (Fig. 4) is calculated by averaging the forces acting on the turbine for each complete rotation. These forces are the force in the direction of the wind motion, F_{Rmov}, and the force perpendicular to the wind motion, F_{Rperp}

$$F_{Rmov} = \sum_{i=1}^{N} \frac{F_{\theta_i} \sin\theta_i + F_{n_i} \cos\theta_i}{2\pi} \Delta\theta \tag{21}$$

$$F_{Rperp} = \sum_{i=1}^{N} \frac{F_{\theta_i} \cos\theta_i + F_{n_i} \sin\theta_i}{2\pi} \Delta\theta \tag{22}$$

and

$$F_R = \sqrt{(F_{Rmov})^2 + (F_{Rperp})^2} \tag{23}$$

Projecting these forces in the x and y directions, we obtain

$$F_{Rx} = F_{Rmov} \cos\left(\gamma + \frac{\beta}{2}\right) + F_{Rperp} \sin\left(\gamma + \frac{\beta}{2}\right) \tag{24}$$

$$F_{Ry} = F_{Rmov} \sin\left(\gamma + \frac{\beta}{2}\right) + F_{Rperp} \cos\left(\gamma + \frac{\beta}{2}\right) \tag{25}$$

14: With this resulting force in the wind direction, the drag coefficient over the rotor can be defined as

$$C_{Drotor} = \frac{F_{Rmov}}{\rho U_\infty^2 A/2} \tag{26}$$

The rotor Reynolds number is defined as [11]

$$Re_{rotor} = \frac{\rho U_\infty^2 D}{\mu} \tag{27}$$

where D is the diameter of the turbine.

15: As the speed of the wind that reaches the turbine (U') is the averaged input speed (U_∞) and the averaged output speed (U_2) on the global control volume [10], U_2 is given by

$$U_2 = 2U' - U_\infty \tag{28}$$

16: Applying the Bernoulli equation [11] between positions 1 and 3 (Fig. 4), the pressure P_3 is obtained

$$P_3 = P_{atm} + \frac{\rho}{2}(U_\infty^2 - U'^2) \tag{29}$$

where P_{atm} is the atmospheric pressure.
Likewise, using the Bernoulli equation between positions 4 and 2 (Fig. 4), the pressure P_4 is also obtained

$$P_4 = P_{atm} + \frac{\rho}{2}(U_2^2 - U'^2) \tag{30}$$

17: From a linear momentum balance [11] applied on the smaller control volume (between planes 3 and 4) and projecting the forces in the x and y directions, we obtain two equations involving two unknown variables, β and γ

$$\vec{F}_R + P_3\vec{A}_3 + P_4\vec{A}_4 = 0 \tag{31}$$

Projecting the forces in the x and y directions, we obtain

$$F_{Rx} = P_4 \sin(90^\circ - \gamma - \beta)A - P_3 \cos(\gamma)A \tag{32}$$

$$F_{Ry} = P_4 \cos(90^\circ - \gamma - \beta)A - P_3 \sin(\gamma)A \tag{33}$$

The variables β and γ can be obtained from Eqs. (32) and (33), as all other variables have already been determined. When we equate Eq. (24) to Eq. (32) and Eq. (25) to Eq. (33), we obtain a nonlinear system of equations. To solve this system, we can use an iterative method. First, we estimate an initial value β' for β. Next, we calculate β as a function of β'

$$\beta = 2\arccos\left(\frac{F_R^2 + (P_4A)^2 + (P_3A)^2}{2P_3A\left(F_R - \frac{P_4A\cos(\beta')}{\cos(\beta'/2)}\right) + 2P_4AF_R}\right) \tag{34}$$

Eq. (34) is solved until the angle β converges assuming $\beta' = \beta$. After calculating β, we calculate γ directly

$$\gamma = \arctan\left(\frac{-F_R\cos(\beta/2) + P_4A\cos(\beta/2) - P_3A}{P_4A\sin(\beta) - F_R(\beta/2)}\right) \tag{35}$$

Certain variables, which are the resultant torque (T), the power coefficient (C_p), the average velocity at the turbine (U') and the velocity at position 2 (U_2), the pressure acting upward (P_3) and downward (P_4) on the turbine and the angles γ and β due to the distortion of the streamlines around the turbine, will be plotted as a function of *tsr* (tip speed ratio), a dimensional variable which is the ratio of the rotational speed of the blade to the free wind speed [15,16]

$$tsr = \frac{\omega R}{U_\infty} \tag{36}$$

With this variable, we can calculate the forces, torque and power for various blade rotational speeds and wind speeds to determine the point of the maximum efficiency.
It is important to stress the viscous effects are taken into account in the integral formulation as well as the experimental results are used together the present theoretical model.

3. Results and discussion

The following data were assumed in order to perform the simulations and to obtain the results presented below. These values were chosen arbitrarily to illustrate the mathematical methodology presented (Table 1).

Figs. 8 and 9 show the lift coefficient and the drag coefficient as a function of the angle of attack of the chosen profile, NACA 0012. This coefficients was obtained experimentally [12].

The following figures present the solutions for the variables of the problem using the presented mathematical model. Fig. 10 shows the velocity U' at which the wind reaches the turbine. This velocity was obtained by applying the iterative method (steps 2–7 of the mathematical model).

Fig. 10 shows that the velocity U' of the wind that reaches the blade follows a periodic function. When the chord of the blade is in the direction of the air flow (90° and 270°), the velocity approaches the free wind velocity (10 m/s). When the chord of the blade is perpendicular to the blade motion (0° and 180°), the velocity of the air at the turbine is minimal. This finding indicates that as the blade chord approaches this position, the air velocity at the blade decreases. It is also shown that the maximum value of the air velocity is the same for all values of *tsr*, and as the *tsr* increases (increasing the angular velocity), the minimum value for U' also increases, i.e., the deceleration of the wind is reduced.

The resulting velocity on the blade and angle of attack are calculated and are shown in Figs. 11 and 12. The velocity on the blade reaches its maximum value at $\theta = 90^\circ$ and its minimum value at $\theta = 270^\circ$, when the wind and the blade move in the same and opposite directions, respectively.

Increasing the *tsr* (thus increasing the rotor angular velocity) increases the resulting velocity of the turbine in the same manner for all positions, as indicated by a displacement of the curve.

Note that in Fig. 12, as the rotation of the rotor increases, the angle of attack decreases [15]. This occurs because the fluid velocity in the tangential direction also increases. Note also that

Table 1
Values of variables used for simulation.

Variable	Value
Free wind speed	$U_\infty = 10$ m/s
Turbine radius	$R = 0.64$ m
Chord length (Profile NACA 0012)	$c = 3.2$ cm
Tip speed ratio	From 4 to 18
Position of the blade	From 0 to 360°
Density	$\rho = 1.19$ kg/m^3
Viscosity	$\mu = 1.84E^{-5}$ kg/(m s)
Atmospheric pressure	$P_{atm} = 1.01325E^5$ Pa

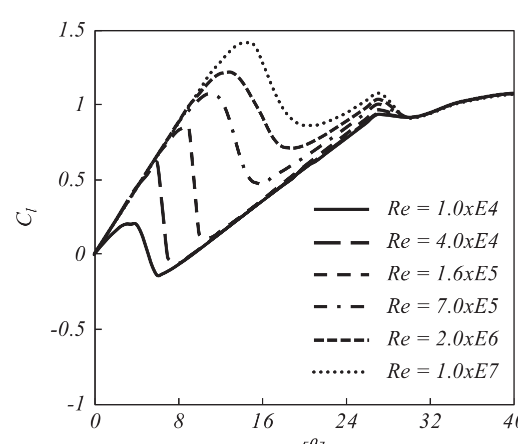


Fig. 8. Experimental lift coefficient (C_l) as a function of the angle of attack (α) of the profile NACA 0012 for various Reynolds number [12].

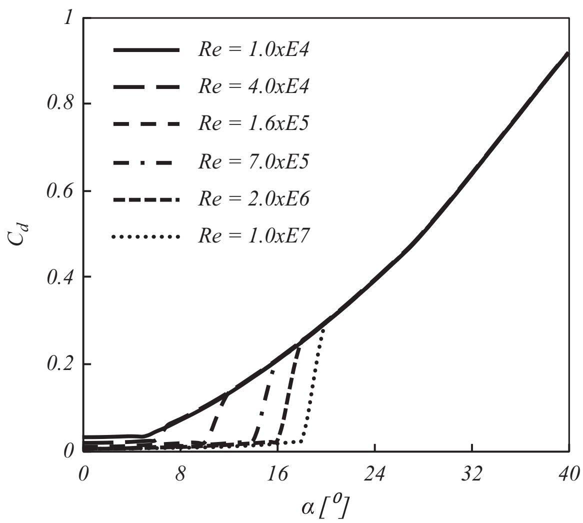


Fig. 9. Experimental drag coefficient (C_d) as a function of the angle of attack (α) of the profile NACA 0012 for various Reynolds number [12].

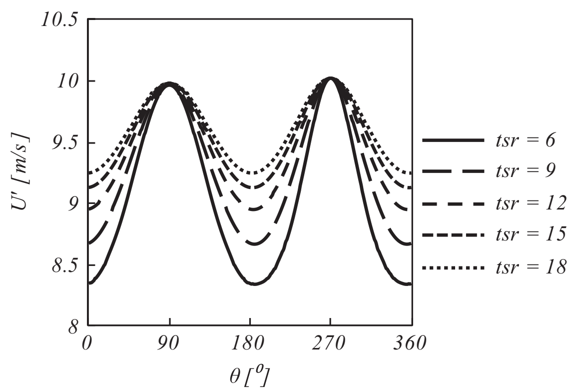


Fig. 10. Wind velocity at the turbine (U') for various *tsr* values as a function of θ.

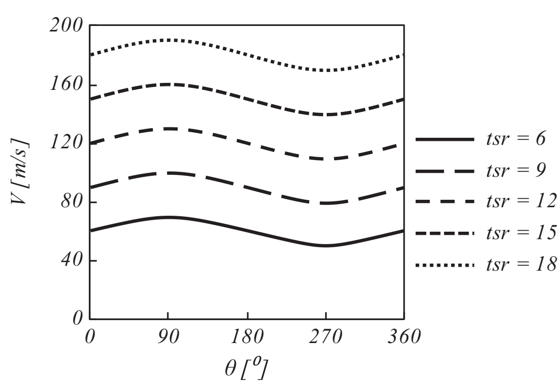


Fig. 11. Resulting velocity on the blade (V) for various *tsr* values as a function of θ.

the angle of attack is zero when the blade is in the direction of the wind velocity, as expected.

Fig. 13 shows the resultant force in the tangential direction. Note that the tangential force is at a maximum when the chord blade is close to the perpendicular direction of the wind (near $\theta = 0$ and 180°); therefore, in these positions, the torque is also at a maximum. When the chord blade is close to the normal direction of the wind ($\theta = 90^{\circ}$ and 270°), the tangential force is minimal and even negative at some positions. However, it is observed that during each cycle, the tangential force is generally positive, and the total torque is therefore also positive.

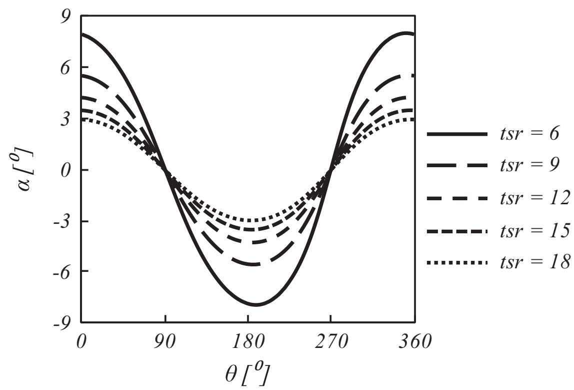


Fig. 12. Angle of attack (α) for various *tsr* values as a function of θ.

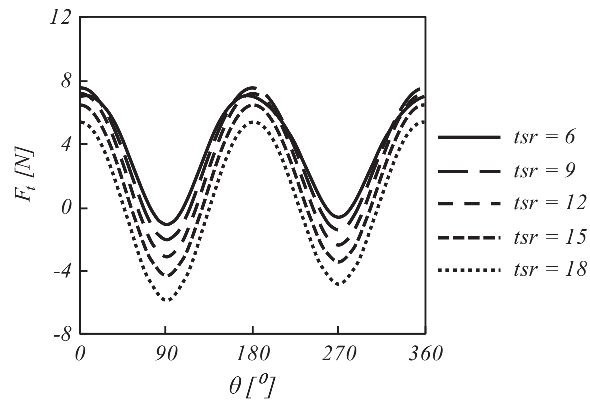


Fig. 13. Tangential force for various *tsr* values as a function of θ.

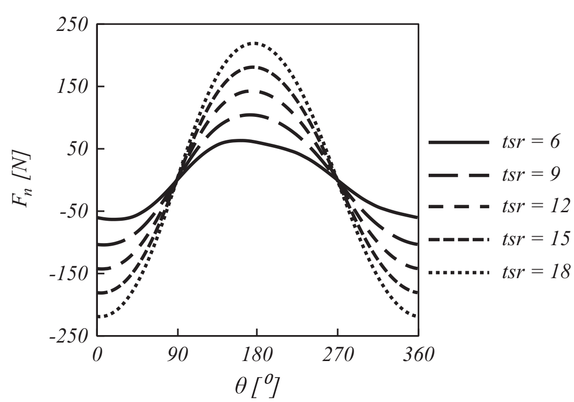


Fig. 14. Normal force for various *tsr* values as a function of θ.

Fig. 14 shows the resultant normal force. This figure shows that the absolute value of the normal force is larger when the chord blade is close to the perpendicular direction of the wind (near $\theta = 0$ and 180°), and smaller when the chord blade is close to the parallel direction of the wind ($\theta = 90^{\circ}$ and 270°). As the angular velocity increases, the normal force also increases. The normal force does not influence the resultant torque but is important in determining the mechanical efforts on the rotor.

Fig. 15 shows the torque (T) generated by the turbine, which was obtained using the average of the tangential force acting on it (Eq. (17)). The torque is bigger for lower values of *tsr*, due to the fact that tangential forces also are bigger for this *tsr* values.

We can also obtain the power (Eq. (18)) and the power coefficient C_p (Eq. (19)), which is shown in Fig. 16.

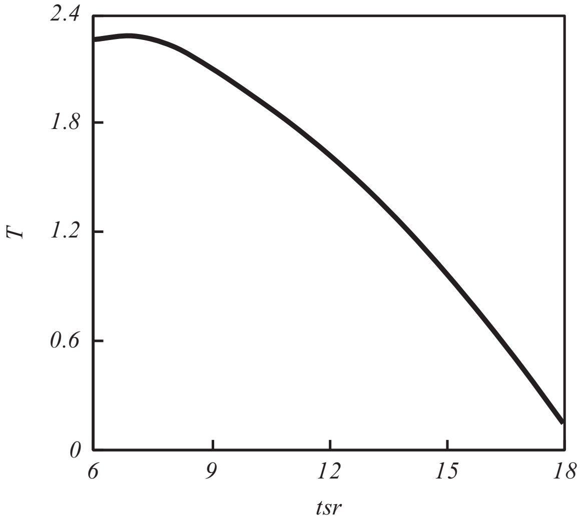


Fig. 15. Torque on the turbine as a function of *tsr*.

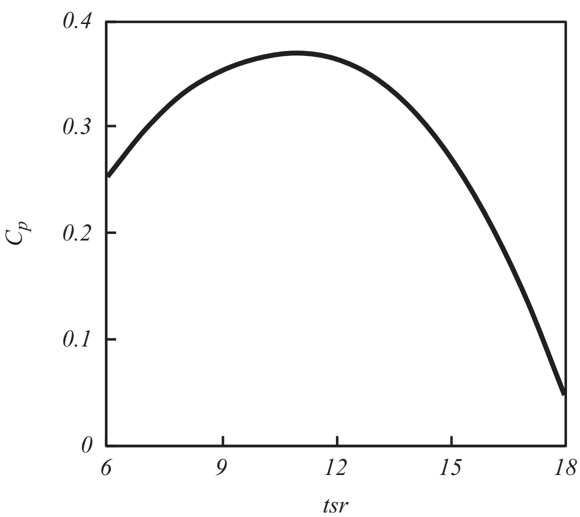


Fig. 16. Power coefficient of the turbine as a function of *tsr*.

The C_p curve obtained obeys the characteristics of this type of turbine. As the *tsr* increases, the C_p increases, reaching a maximum before decreasing. In this simulation, the maximum C_p is near 0.35 for a *tsr* near 11. It can also be observed that the power coefficient does not reach the Betz limit, which is 0.59 [10], as expected.

Fig. 17 shows a comparison between the three velocities: the free stream wind velocity (U_∞), the average velocity at the turbine (Eq. (11)) and the velocity at position 2 (Fig. 5) of the larger control volume (U_2, Eq. (28)).

The velocity of the wind reaching the turbine increases as the turbine rotation increases, and when the angular velocity approaches infinity, the average velocity approaches the free stream wind velocity. The velocity at point 2 is less than U' and is directly proportional to the velocity at the turbine. The curve shows that the air velocity at the turbine is the average of the free stream wind velocity and the velocity at position 2.

Fig. 18 shows the averaged forces acting upon the turbine during one complete rotation. After averaging the forces during one complete rotation, we see that the force in the direction perpendicular to the motion of the fluid is zero, leaving only the force in the direction of the air movement. This force increases linearly with the angular velocity.

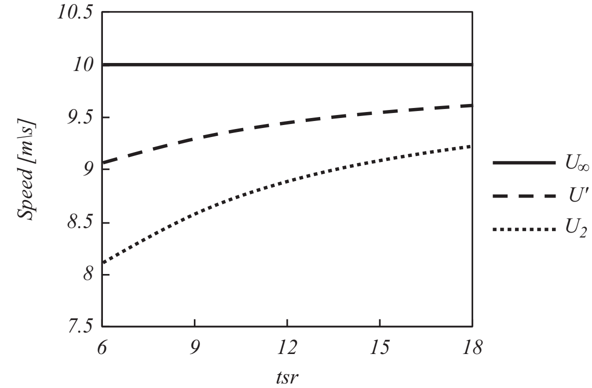


Fig. 17. Resulting velocities as a function of various *tsr* values.

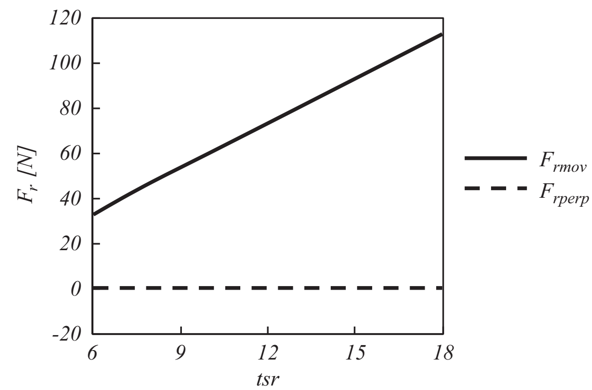


Fig. 18. Resulting average forces for various *tsr* values.

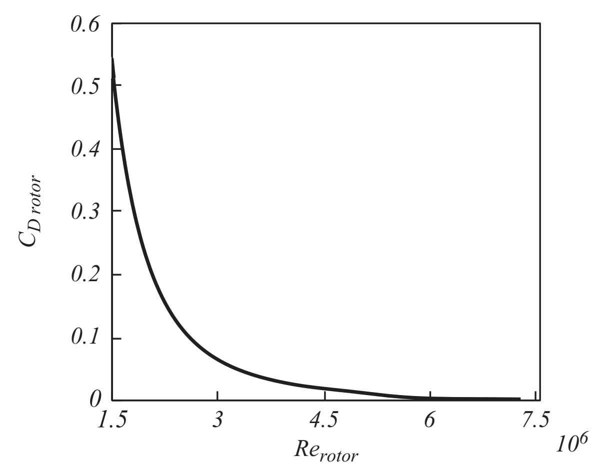


Fig. 19. Drag coefficient over the rotor as a function of the Reynolds number.

Fig. 19 shows the drag coefficient over the rotor as a function of the Reynolds number. The drag coefficient decays nonlinearly, as expected. This decay occurs because the drag coefficient on the rotor is proportional to the drag force, which increases linearly and is inversely proportional to the square of the wind speed.

Fig. 20 shows the pressure acting upward (P_3) and downward (P_4) on the turbine and the atmospheric pressure. It is observed that the pressure P_3 before the turbine is above atmospheric pressure and the pressure P_4 after the turbine is below atmospheric pressure. This is due to the drag generated by the turbine. Note also that the pressure decays before the turbine and increases after the turbine as the *tsr* increases. When the speed

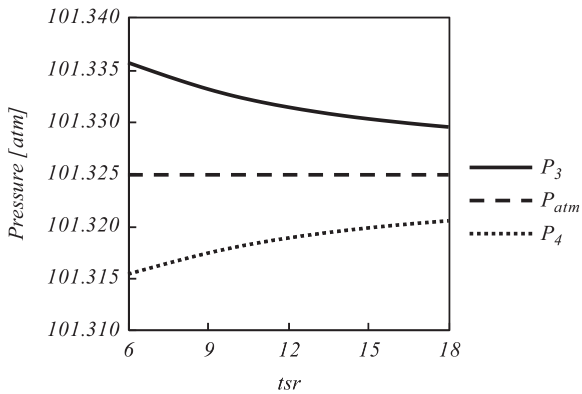


Fig. 20. Pressures distributions for various *tsr* values.

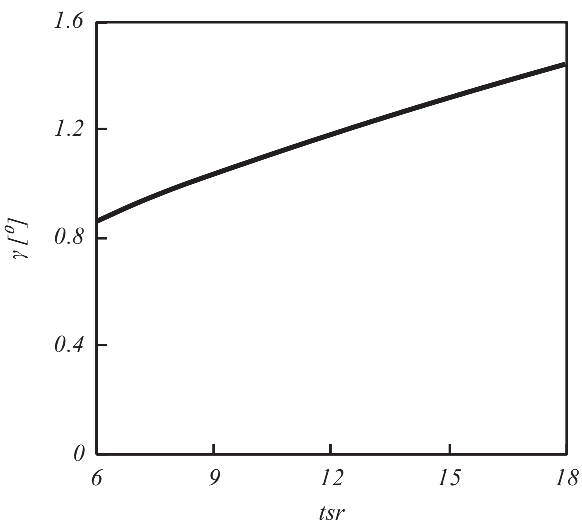


Fig. 21. Pressures distributions for various *tsr* values.

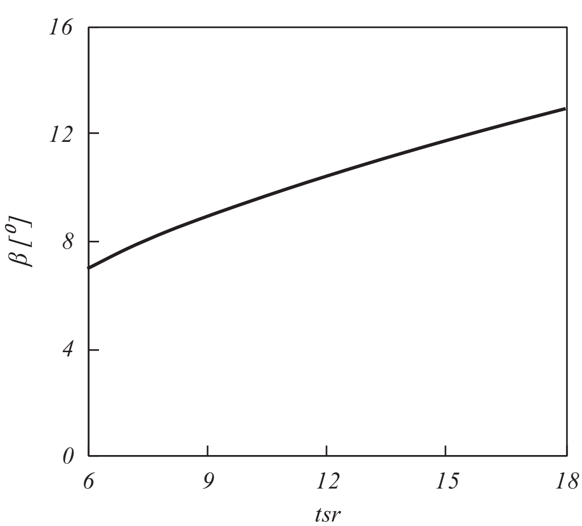


Fig. 22. Pressures distributions for various *tsr* values.

ratio approaches infinity, the pressure before and after the turbine approaches the atmospheric pressure.

Figs. 21 and 22 show the angles β and γ due to the distortion of the streamlines around the turbine. It is expected that as the angular velocity decreases, the streamlines display less distortion, and when the rotation angle is zero, both angles approach zero. Otherwise, the higher the angular velocity, the greater the distortion of the streamlines.

4. Conclusion

Wind energy is part of the solution to the world's energy demands. Computational analysis for wind turbines is notably versatile, as it avoids the costs of experiments and projects in physical facilities, and it can easily simulate and handle variable changes to seek the best solutions.

With a full analysis for given wind conditions, it is possible to choose a good aerodynamic profile for a turbine. The angular velocity of the axis can be chosen such that the turbine operates near its maximum efficiency.

With the coefficient of total drag on the rotor and the angles of distortion, it is possible to perform a global analysis of the flow in a wind farm. We can determine the minimum distance required between two turbines to guarantee that the air flow passing through the first turbine approaches the velocity and pressure of the free wind before passing through the next turbine.

Nevertheless, the integral analysis requires empirical inputs for each type of rotor blade. In order to avoid this requirement, computational fluid dynamics methods can be useful. This subject is the next step and the focus of the continuation of the present research.

Acknowledgments

The authors are grateful to FAPEMIG, CNPq and PETROBRAS for providing financial support.

References

[1] Ibenholt K. Explaining learning curves for wind power. Energy Policy 2002. http://dx.doi.org/10.1016/S0301-4215(02)00014-9.
[2] Islam M, Ting DS-K, Fartjar A. Aerodynamic models for Darrieus-type trainght-blades vertical axis wind turbines. Renewable and Sustainable Energy Reviews 2006. http://dx.doi.org/10.1016/j.rser.2006.10.023.
[3] Camporeale SM, Magi V. Streamtube model for analysis of vertical axis variable pitch turbine for marine currents energy conversion. Energy Conversion and Management 1999. http://dx.doi.org/10.1016/S0196-8904(99)00183-1.
[4] Blackwell BF. The vertical-axis wind turbine how it works. Technical report SLA-74-0160. Sandia National Laboratories, Albuquerque, NM, EUA; 1974.
[5] Vertical axis wind turbine, the history of the Doe program; 1999.
[6] Templin RJ. Aerodynamic performance theory for the NRC vertical axis wind turbine. Technical report LTR-LA-160, NCR of Canada TR; 1974.
[7] Strickland JH. The Darrieus turbine: a performance prediction model using multiple streamtubes. Technical Report SAND 75-041, Sandia National Laboratories, Alburquerque, NM, EUA; 1975.
[8] Paraschivoiu I. Double-multiple streamtube model for Darrieus wind turbines. In: NASA Conference Publication 2185. 1981.
[9] Janajreh I, Qudaih R, Talab I, Ghenai C. Aerodynamic flow simulation of wind turbine: Downwind versus upwind configuration. Energy Conversion and Management 2010. http://dx.doi.org/10.1016/j.enconman.2009.12.013.
[10] Betz A. Windmills in the light of modern research. Technical report. National Advisory Committee for Aeronautics, Washington, EUA; 1928.
[11] Çengel YA, Cimbala JM. Mecânica dos Fluidos Fundamentos e Aplicações. McGraw-Hill Interamericana do Brasil Ltda; 2007.
[12] Sheldahl RE, Klimas PC. Aerodynamic characteristic of seven symmetrical airfoil sections through 180-degree angle of attack for use in aerodynamic analysis of vertical axis wind turbines. Technical report SAND 80-2114. EUA, Sandia National Laboratories, Alburquerque, NM, EUA; 1981.
[13] Sharma RN, Madawala UK. The concept of a smart wind turbine system. Renewable Energy 2011. http://dx.doi.org/10.1016/j.renene.2011.08.051.
[14] Sheldahl RE, Klimas PC, Feltz LV. Aerodynamic performance of a 5-metre-diameter Darrieus turbine with extruded aluminium NACA-0015 blades. Technical report SAND 80-0179. EUA, Sandia National Laboratories, Alburquerque, NM, EUA; 1980.
[15] Degraire P. Analytical aerodynamic simulation tool for vertical axis wind turbines. PhD thesis. Uppsala Universitet; 2010.
[16] Kjellin J, Bulow F, Eriksson S, Deglaire P, Leijon M, Bernhoff H. Power coefficient measurement on a 12 kw straight bladed vertical axis wind turbine. Renewable Energy 2010. http://dx.doi.org/10.1016/j.renene.2011.03.031.